Design of Adaptive Autoreclosure Schemes for 132 kV With High Penetration of Wind—Part II: Real-Time Development and Testing

Simon P. Le Blond, *Member, IEEE*, and Raj Aggarwal, *Senior Member, IEEE*

***Abstract*—Following part 1, this paper describes the development and real-time testing of an adaptive autoreclosing scheme for a 132-kV system with high penetration of wind generation. Having previously established the real-time system model, this second part concentrates on the hardware and software tools used to build the relay development platform, the algorithm itself, and the testing of this algorithm. A results section documents tests of the neural–network-based algorithm and is shown to be 100% reliable. Further successful tests on a 400-kV system suggest that the algorithm is robust to other system configurations.**

***Index Terms*—Adaptive reclosing, power system protection, real-time simulation, transmission lines, wind generation.**

I. Introduction

FOR THE purposes of this paper, adaptive autoreclosing (AA) on overhead lines is the ability to distinguish between a transient or permanent fault following a short circuit, and then issue a reclose signal if and only if the transient fault no longer exists. This approach is beneficial for quickly restoring supply, increasing system stability, and minimizing secondary shocks to the system due to unsuccessful reclose attempts. Single-phase adaptive autoreclosure takes advantage of around 80%–90% of overhead line faults being transient and 70%–90% involving a single phase to ground [1]. It therefore demands correct phase selection and the ability of the circuit breaker to open a single phase, and leave the healthy phases intact. A permanent fault has a constant fault resistance since it usually involves a physical short circuit, due to vegetation, downed line, or broken conductor. In contrast, a transient fault involves arcing across the arcing horns and is usually caused by lightning or adverse weather conditions. The heavy current primary arc before the circuit breaker opens is difficult to detect because although the resistance is dynamic, it stays in the order of a few ohms, similar to the permanent fault. Following the single-phase breaker opening, the healthy phases (those that remain energized) mutually couple and drive a highly nonlinear, lower current secondary arc on the faulted phase. When this arc eventually extinguishes, it is safe to reclose the circuit breaker and bring the line back into normal service.

The notable difference between secondary arcing and a permanent fault gives rise to the possibility of robust diagnosis between the two cases. However, there is a complex interplay of parameters that determine both voltage signatures, some of which cannot be known prefault. It is therefore problematic to rely solely on power frequency measurements. In the past, researchers have addressed this problem a number of ways, including signal processing and neural networks [2], fuzzy logic and wavelet transforms [3], and straightforward numerical techniques [4]. These methods all rely on the higher frequencies caused by the secondary arc. However, only the artificial-neural-network (ANN) technique has been deployed on a real system and documented in the literature [5] and, therefore, forms the basis of this algorithm.

In recent years, the U.K. has seen a considerable increase in wind power in the generation mix, and around half of this installed capacity is currently onshore [6]. Modern variable speed turbines involve power electronics in the ac/ac conversion process to export power at the desired grid frequency. This is usually in the form of a back-to-back converter whose individual gates are pulsewidth modulated. The result of this approach is the injection of harmonics onto the local grid. Filters are therefore required to eliminate lower order harmonics so that utility grid codes are met. One concern about wind farm power quality (PQ) is its effect on transient-based protection, such as AA, due to the latter relying on higher frequencies.

The primary purpose of this paper is to assert the conclusions drawn in [7] that, in fact, AI autoreclosing techniques are robust to the presence of wind farms. This is achieved by demonstrating an ANN-based AA scheme in real time on a transmission line adjacent to a wind farm. The real-time platform used is described in the earlier paper [8]. This paper concentrates on the real-time hardware, software, and the algorithm itself.

Seldom in the literature are novel protection algorithms demonstrated in real time and hardware in the loop control. The secondary purpose of this paper is to describe a low cost, versatile relay development platform achievable within an academic environment. The authors believe that such an approach may greatly hasten commercialisation of academic research output in power system protection.

II. Problem Space

The task of adaptive autoreclosure is, in essence, one of pattern recognition. Fig. 1(a) shows a transient fault and Fig. 2(b)

Manuscript received May 04, 2011; revised August 21, 2011; accepted August 31, 2011. Date of publication October 25, 2011; date of current version June 20, 2012. This work was supported by the EPSRC led SUPERGEN:FLEXNET consortium. Paper no. TPWRD-00276-2011.

The authors are with the Centre for Sustainable Power Distribution, Department of Electronic and Electrical Engineering, University of Bath, Bath BA2 7AY, U.K. (e-mail: S.P.Le.blond@bath.ac.uk).

Digital Object Identifier 10.1109/TPWRD.2011.2168571

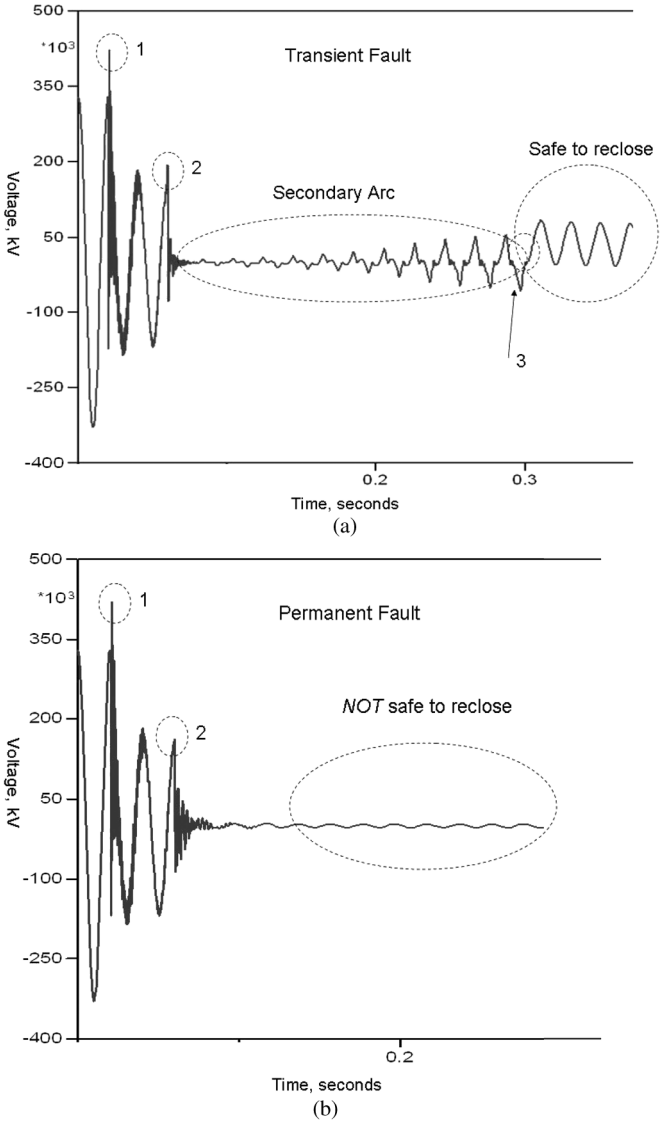

Fig. 1. (a) Faulted phase voltage time series of a transient fault. (b) Faulted phase time series of a permanent fault. These figures show the cases that the adaptive autoreclosing relay must differentiate between.

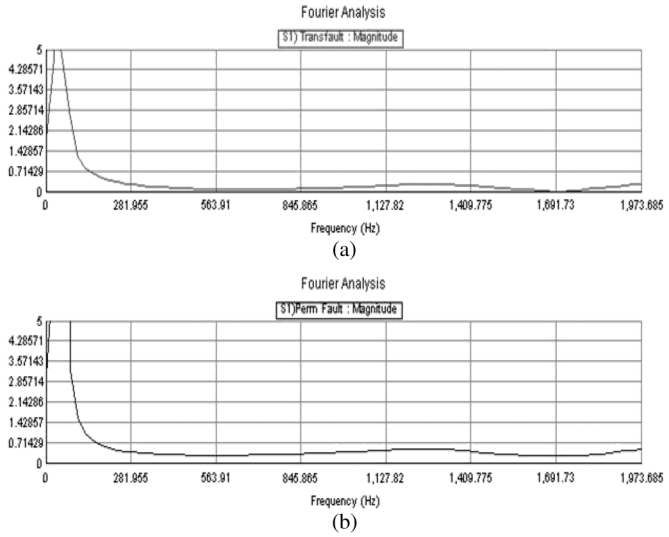

Fig. 2. Frequency-domain plots of the primary arcing period (2a) against the permanent fault (2b) from 0–2 kHz. The similarities make precircuit breaker fault diagnosis hard to achieve.

shows a permanent fault time series for a 400-kV system generated by Electromagnetic Transients Program–Alternate Transients Program (EMTP-ATP) draw. These are taken from the line side of the breaker on the faulted phase, being essentially what the relay "sees," albeit via the CVT, or other transducer, in order to transform to practical secondary system voltages. The arc models are described fully in [9].

At point 1 on Fig. 1(a), the transient arcing fault occurs. The protection signals the circuit-breaker operation at point 2 and the secondary arc begins, which eventually extinguishes, leaving a plain permanent sinusoid. In Fig. 1(b), the same sequence of events occurs, except the resistance of the fault is fixed. After point 2, the circuit breaker operates, and after a short period of transients, a bare permanent sinusoid remains.

In terms of the autoreclosing problem, there are two important conclusions to draw from Fig. 1(a) and (b). The voltage trace between 1 and 2 shows very little variation and, thus, renders diagnosis between fault types difficult in this period, discussed further in Section II. In addition, the postarcing period in Fig. 1(a) and the permanent fault Fig. 1(b) are both plain sinusoids, but belong to different classes in the problem space. In the technique described by Fitton *et al.* [2], a single ANN is used to diagnose between *safe to reclose* or *not safe to reclose* conditions with respect to the time series. An important innovation on this method is to assign two neural networks, A and B, separate tasks. A is assigned the task of arc fault-type determination and B is assigned the task of arc extinction. This means that reclosure is only sanctioned by the arc extinguish network if the type detecting network has deemed the fault to actually be transient. This increases the robustness of the method, through the "divide and conquer" approach, because the networks are "experts" at their designated tasks.

III. Arc Model

The arc model is possibly the most important aspect of the simulation in the 132-kV system. This is necessary to model the dynamic fault resistance associated with the transient arcing fault. The arc conductance is described by (1), the equation for unconstrained arcs in air

$$\frac{dg}{dt} = \frac{1}{\tau}(G - g) \tag{1}$$

where in (1), G is the stationary arc conductance, g is the time dependent arc conductance, and is τ the time constant. These parameters are themselves dependent on various others that are empirically determined by volt-current cyclograms [10], [11]. The behavior of the arc occurs in two distinct stages, before and after the circuit breakers open. The primary arc is a heavy current, high-energy arc, fed by the short circuit on the associated phase conductor. In this stage, the arc length does not evolve appreciably with time and the average resistance is in the order of a few ohms, similar to a permanent fault resistance. This similarity to a permanent fault renders the phenomena extremely difficult to diagnose with conventional transducers. A technique has been proposed [12], but it relies on line traps to detect very

high frequencies. The RTDS system guarantees fidelity of up to 3 kHz, but the frequency response of most conventional CVTs is only faithful to about 700 Hz [9]. The frequency response begins to attenuate after this since the CVT equivalent circuit acts like a low-pass filter. It is therefore only realistic in this context of real-time simulation to make a robust diagnosis using the secondary arcing period. Fig. 2(a) and (b) shows the similarity in the frequency domain between the permanent fault and the primary arc up to 2 kHz, showing why it is not feasible to use frequency-domain information for such purposes.

Fig. 2(a) and (b) were produced with the precompiled fault arc model in the draft library of the RSCAD software. A detailed explanation of how the RTDS arc model is achieved is available in [13] but briefly, the integrator control blocks solve (1) for arc conductance on a per time-step basis. The evolution of secondary arc length is controlled by random white noise and Gaussian noise generators. This helps keep a realistic element of randomness to the arc signature and means that no two test runs are identical. Reference [13] shows that the model gives good agreement with real-world fault tests. In this work, a permanent fault is represented by a permanent resistance of 2 Ω to ground, except when this parameter is varied for testing purposes.

IV. Algorithm

This sample rate is set to 20 kHz and the input sample rate from the RTDS is then downsampled to 2.5 kHz, forming the input time series to the algorithm shown in Fig. 3. (The data-acquisition module, the X3-SD, has an oversampling facility and internal antialiasing filters.) The downsampling makes the size of the frequency transform per timestep much less computationally onerous. The time-domain information is then fed to a 64-sample buffer. The buffer is Hann windowed and the resultant subjected to the fast Fourier transform (FFT). The purpose of the Hann window is to minimize edge effects and weigh the window so that the frequencies in the center have the maximum influence. The frequency bands are 39.1 Hz wide. This captures the power frequency component as well as giving the best FFT frequency resolution. Extensive simulations show that in the secondary arcing period on the transient fault, only the first eight frequency bands show significant information, up to around 300 Hz. Fig. 4 shows a 3-D spectrogram *looking back across the time axis*. (This perspective makes the secondary arcing frequencies easier to observe.) Only the first eight frequency bands are used and the rest are discarded. The time-varying magnitudes over these eight frequency bands form the input layer of two multilayer perceptrons. However, the frequency boundaries must undergo an important intermediate stage of input scaling and clipping. This serves to normalize all inputs to the multilayer perceptron between 1 and −1. The upper and lower bounds to each frequency band $\mathrm{X_{max}}$ and $\mathrm{X_{min}}$ are determined offline by secondary arc training waveforms. The transfer function may be summarized by

$$Y_{\mathrm{out}} = f(x) = x\left[\frac{2}{X_{\mathrm{max}} - X_{\mathrm{min}}}\right], \quad \mathrm{X_{min}} < \mathrm{x} < \mathrm{X_{max}}$$
$$Y_{\mathrm{out}} = 1, \quad \mathrm{x} > \mathrm{X_{max}}$$
$$Y_{\mathrm{out}} = -1, \quad \mathrm{x} < \mathrm{X_{max}}. \tag{2}$$

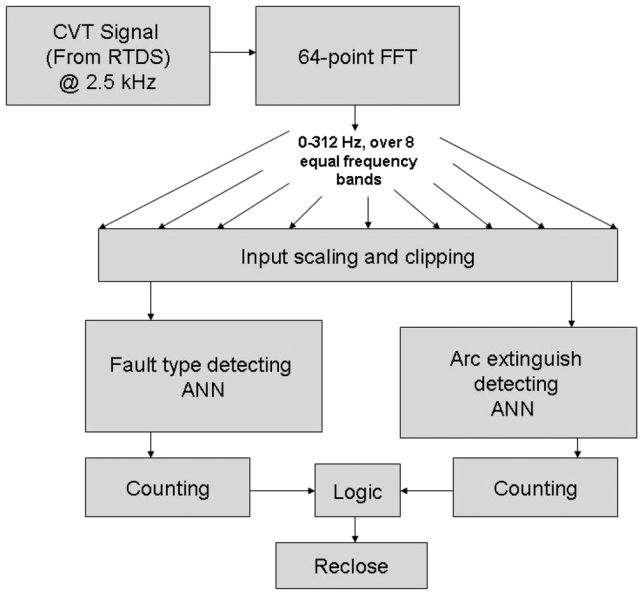

Fig. 3. Simplified block diagram showing how the CVT signal is processed to arrive at a trip decision. An arc must be detected *and* extinguished to arrive at a trip decision.

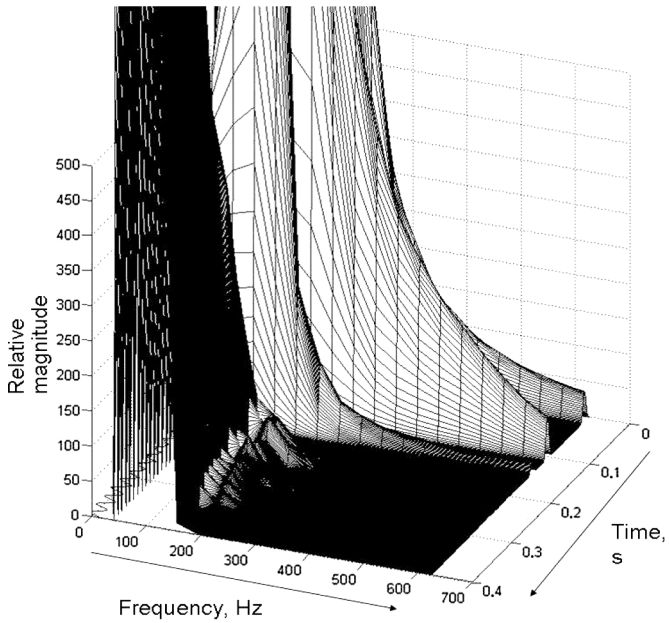

Fig. 4. A 3-D spectrogram showing how the faulted phase voltage varies in the frequency and time domain, looking back across the time axis. The front axis shows frequency. The secondary arc begins at about 0.15 s, and only the frequencies up to 300 Hz are particularly significant thereafter.

V. Multilayer Perceptron

The computing tool at the heart of the algorithm is an artificial neural network (ANN), specifically, of multilayer perceptron (MLP) architecture. MLPs are feedforward networks, trained using supervised learning techniques. They are capable of discerning nonlinearity, can recognize trends in data and are robust to noise. They use supervised learning algorithms to adjust their synaptic weights so that they respond in the desired manner for similar input data. The ANNs are fed eight input frequency bands from the discrete time series sampled from the secondary

arc voltage. The input is then routed through the hidden layer onto a single output neuron that indicates the binary diagnostic task it has been trained for. The algorithm presented uses two ANNs. One network diagnoses the presence of the arc while the other diagnoses the arc extinguish. The networks were developed in MATLAB's Neural Networks toolbox.

Both networks consist of an 8-12-1 architecture, that is, 12 hidden layer neurons. Various architectures were tried, but most trial ANNs performed equally well. Within wide limits, the size of the hidden layer did not significantly influence the network's ability to perform their designated task in this application. Taking guidance from [9], an average network size was therefore chosen in an attempt to ensure the algorithm was robust against primary system variation. The robustness is due to a well-defined problem space in both cases: the fault type and extinguish are both easily characterized by an abundance, or lack thereof, of higher frequency components in the 50–300 Hz bands. The transfer functions in the hidden layer and the output layer were selected to be logistic sigmoid and the training algorithm was Matlab's resilient back propagation. The output neuron is trained to output a zero or one indicating in which class the input time series belongs. This method is adapted from the technique described in [2]. In practice, the output of each ANN is never precisely 1 or 0, however, so an output above a threshold of 0.5 is rounded to indicate 1 and below 0.5, to indicate 0. Clearly, each decision cannot be based on a single windowed FFT, as this would not be particularly robust. The network does occasionally swing into the wrong domain due to frequency anomalies. In the case of the arc extinguish ANN, this is compounded by a dither region when the secondary arc extinguishes. Over this period, the windowed FFT takes both information from the *not safe to reclose* and the *safe to reclose* periods. This is avoided in the ANN training cases, but cannot be avoided when the algorithm is deployed online since no previous knowledge exists of when the arc extinguish will occur. To increase robustness, a counting mechanism is introduced so that both ANNs must have a consistent output of above 0.5 for a full power system cycle before a decision is reached. In the case of the fault type ANN, the decision is framed so that the counter must register an arcing fault or the fault is assumed to be permanent, thus minimizing the chance of reclosing onto an arcing fault. In practice, the marked difference between the arcing fault and the permanent fault means that the fault is always correctly diagnosed well before any existing arc extinguishes.

A computational load assessment in [15] suggests that the FFT costs about 3 times more floating point operations per second (FLOPS) than the ongoing evaluation of both neural networks. The total computational load of the algorithm, at maximum theoretical efficiency, is about 3 MFLOPs. A single core of the Intel I5 processor, on which the scheme is tested, is capable of more than 20 GFLOPs, over 6×10^3 times faster.

Fig. 5(a) shows a typical time-domain response of the ANNs to a transient fault and Fig. 5(b) is the response to a permanent fault. The middle trace on both figures shows the arc extinguish detecting ANN and the last trace, the type detecting ANN. In the case of Fig. 5(b), the second trace is ignored by the algorithm since the fault is correctly diagnosed as permanent. In other words, there is no arc extinguish to detect.

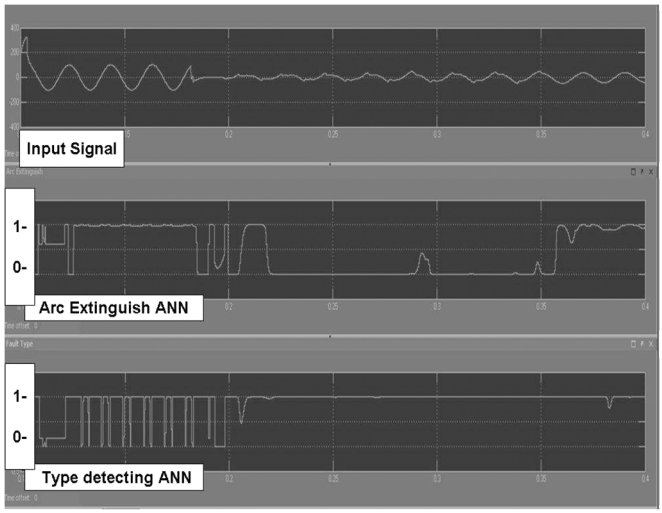

(a)

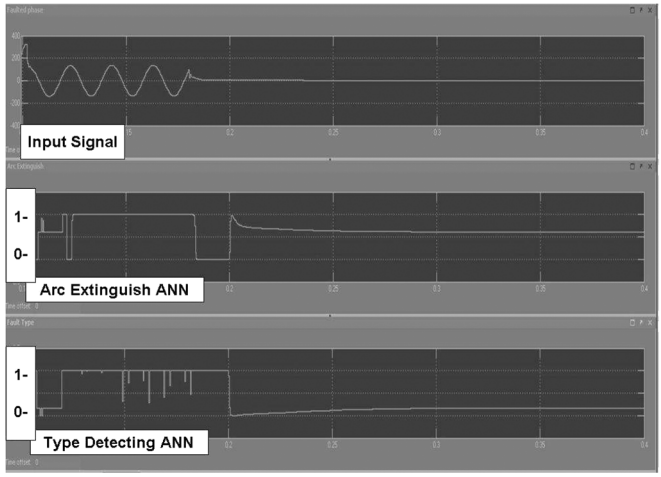

(b)

Fig. 5. (a) Typical time-domain ANN response to a transient fault. (b) Typical time-domain ANN responses to a permanent fault. The middle trace in this case is not used since the fault is correctly diagnosed as permanent.

VI. Pseudorelay Development and Test Platform

The purpose of the pseudorelay platform is to provide an authentic system that can be decoupled from the RTDS, receiving analog system inputs in much the same way a substation relay would from a CVT. The possibility of digital in also makes the platform potentially capable of IEC 61850-compliant interfacing. The onboard data-acquisition module with built-in field-programmable gate array (FPGA) turns the PC into a versatile prototyping station with considerable processing power. Using this approach, any problems in the development stage, such as prohibitive computational overheads or robustness, are overcome, making commercialisation more attractive to a necessarily conservative industry. Fig. 6 is a block diagram showing the real-time development platform as well as indicating how

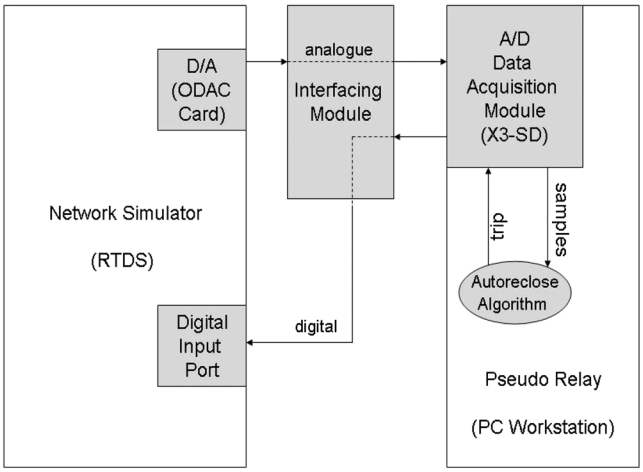

Fig. 6. Block diagram of the real-time development platform.

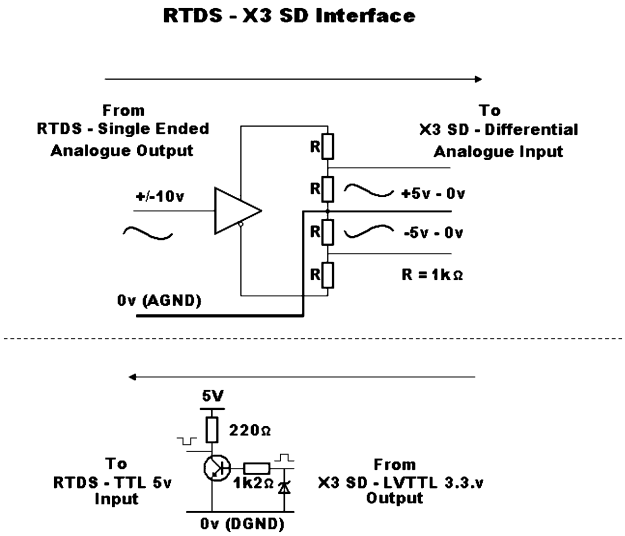

Fig. 7. Single-channel circuit diagram of the interface box. The first circuit is an analog channel to the pseudo and the second is a digital from the pseudorelay to the RTDS. The $+/-12$-V supply rails are omitted for clarity.

the pseudorelay system connects to the RTDS. The data-acquisition module is innovative integration's X3-SD, a 16-channel, hi fidelity analog capture board with an onboard 1 M gate FPGA. This streams samples in packets to the workstation via a PCI express bus. Sample rates of up to 216 kHz per channel are possible and streaming data rates to the host of up to 100 MB/s are achievable. The purpose of the interfacing module is to convert analog signals from the RTDS ODAC out to acceptable input levels for the X3-SD analog-to-digital module. The interfacing module also brings digital out from the analog to digital up to acceptable levels. A circuit diagram of the X3 SD interface is shown in Fig. 7.

With reference to Fig. 7, the RTDS ODAC cards supply a single-ended ac signal with a peak voltage of $+/-10$ V. The X3-SD operates best on a differential signal, where each differential pair must be $+/-5$ V peak. This arrangement rejects any common-mode noise, producing a cleaner signal. It is therefore necessary to use a differential driver coupled with a potential divider circuit in the arrangement shown in Fig. 7. In the reverse direction, the reclose signal is sent to the X3-SD with digital logic. The digital out of the X3-SD runs on 3.3-V logic whereas the digital input ports of the RTDS operate on 5-V logic. The digital input ports of the RTDS are inverted, so that 0 V indicates a logical 1. A transistor is therefore wired as a switch, so that 3.3 V supplied to the base will result in 0 V between the emitter and collector. The Zener diode ensures that the input signal to the transistor can never exceed much more than 3.3 V.

The development platform is equipped for 12 channels of analog in and four channels of digital out. In theory, all voltages and currents from a three-phase double-circuit line may be used for inputs to any prototype relay, or for that matter, 12 signals from anywhere in the primary system. It should be stated explicitly, however, that the AA algorithm only uses two channels of analog in, namely, the faulted phase and circuit-breaker status, and a single channel of digital out to indicate a reclose event. Following the circuit-breaker operation, and consequent initiation of the secondary arc, the second channel of analog triggers the algorithm. This approach ensures that the ANNs only act on the secondary arc and not the steady-state signal, as they have not been trained to deal with the latter.

VII. Software

The X3-SD is supplied with an extensive C++ class library known as *Malibu*. The *Malibu* library allows the user to develop custom applications to process the data as it is captured and streamed to the host. An example program *SNAP* that configures, arms, and executes data capture is also bundled as a *Microsoft Visual Studio* project, along with support for various other development environments. The user may augment the source code with Malibu and recompile the program to suit his or her specifications.

The algorithm was developed with Mathwork's ubiquitous engineering software *MATLAB*. In MATLAB, SIMULINK's embedded real-time encoder was used to code block models into C++. This approach considerably speeds up development time as SIMULINK models can be directly coded for prototype targets, tested, and then quickly adjusted if required.

The Simulink-generated source code was imported to the SNAP project as a stand-alone method that could be invoked from the main program for every algorithm time step. Each time a sample is received from the RTDS, this method (i.e., the SNAP project method) is called up, with the sample's value as the input to the method. As mentioned in Section IV, it is necessary to downsample the input to make the FFT yield the required frequency resolution. This downsampling is achieved within the algorithm, with the SNAP sample rate set to 20 kHz, and the algorithm's code discarding seven samples in every eight. As mentioned earlier, an antialiasing filter is applied by the X3-SD. As can be seen in Fig. 4, the amplitude of secondary arc frequencies above 400 Hz is insignificant relative to those below, so it was not necessary to apply a second low-pass filter after the downsample. The method was set to return the circuit breaker status and link to the Malibu digital out class function, so that a 1 was sent to the digital out channel when the algorithm computed a reclose to be necessary. This signal is sent to the RTDS via the interface module.

VIII. Training and Testing

Previous studies [14] have shown that the postfault transient voltage is responsive to the following parameters: system voltage, line length, geometric line configuration, bus short-circuit capacities, fault point on line, fault inception point on the waveform, and permanent fault resistance. Of these, the last three parameters are not known prefault and so cannot be configured before the relay is deployed on any real-world system. These parameters were therefore varied over the test cases to test the algorithm for its sensitivity to them.

Any algorithm using ANNs must involve training the ANNs to respond appropriately to their input data. This is most effectively achieved by using fault waveforms generated by varying each relevant parameter over the full range of values the scheme will encounter in practice. In a real-world fault scenario, each parameter may take any value on a continuous range. However, in producing the training set, it is only practical to vary each parameter in large, discrete steps. This is because a large number of parameter permutations quickly combine to produce a prohibitively large training set. The RTDS model provided training and test cases, but there were important differences in the model used for training and the model used for testing. This was to ensure that the ANNs could generalize rather than simply memorize (i.e., to ensure that they were able to recognize trends in test data rather than just reproduce their performance). Moreover, the integral reason for establishing the realistic primary system model described in part 1 [8] was to determine the algorithm's sensitivity to the presence of wind generation. Therefore, parameters to generate the training and test cases were varied as shown in Table I, with the training cases denoted by column A and the test cases column B. The test cases that used a different primary system model are discussed in the next section.

It should be mentioned that the initial fault inception angle had no significant bearing on the secondary arc other than determining where it began, and only because the response time of the breaker was fixed by the simulation. However, the algorithm ignored the first cycle after the circuit-breaker operation to allow the circuit-breaker transients to attenuate. For this reason, it was not necessary to vary the fault inception angles between the training and test cases.

When staging fault tests, it is necessary to split the line model into two sections with a "virtual bus" in the center, where the fault may be grounded to simulate a single-phase-to-ground fault. Unless the line is split equally, splitting a 30-km transmission line will result in one line section being shorter than 15 km. In the test sets, such sections must be represented with a simple PI model, rather than a travelling-wave model, because the travel time is below the fixed RTDS time step of 50 μs. However, the good performance of the algorithm with both model types suggests it is not sensitive to this approximation.

Due to the inherent randomness in the arc model, specifically evolution of the secondary arc length, no two transient fault-test runs are identical. In practice, other parameters are more significant, and the secondary arc extinguish is usually within one cycle of a subsequent run with the same settings.

IX. Real-Time Testing

Fig. 8 shows a typical real time reclose sequence, as observed by the response of the faulted phase CVT voltage. The breaker recloses about 2.5 cycles following secondary arc extinction, and the system is restored to its nominal voltage.

Conversely, Fig. 9 shows a typical response to a permanent fault. In this case, autoreclosure is not sanctioned and voltage is not restored since the fault is correctly diagnosed to be permanent.

TABLE I
Training and Testing

Parameter	Training cases Total: 45	A Test cases Total: 255	B Test cases Total: 147
System Voltage	132 kV	132 kV	400 kV
Bus Short Circuit Capacities	Fixed	Fixed	Fixed
Line Length	30 km	30 km	50 km
Geometric Line	Fixed	Fixed	Fixed
Fault point on line % line length from relay	100% 50% and 0%	0, 16.6%, 33%, 66% and 83.40%	2km intervals transient fault and 10km intervals permanent fault
Inception angle on waveform	90°, 30°, 0°.	90°, 30°, 0°.	90°, 30°, 0°.
Perm fault resistance	0, 2, 50, 100 Ω	0,1, 35, 80 Ω	0, 1, 35, 80 Ω
Wind Farms at Farr and Paul's Hill	No, voltage source behind equivalent subtransient reactance	Yes	N/A

Table I shows how parameters were varied to generate the training and test cases.

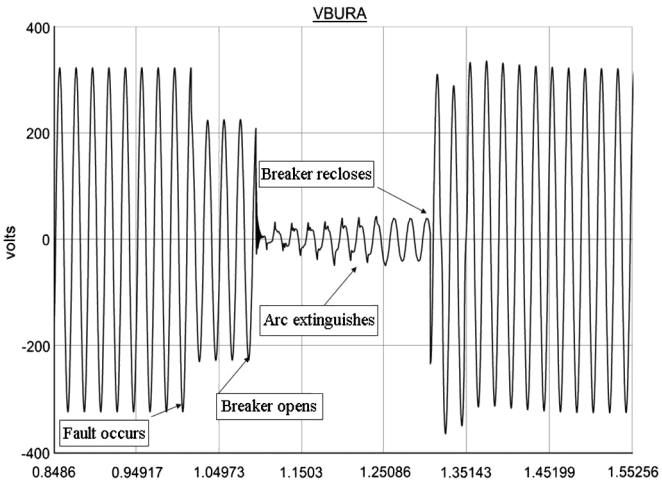

Fig. 8. Typical real-time response to a transient fault, the faulted phase voltage viewed via the CVT output.

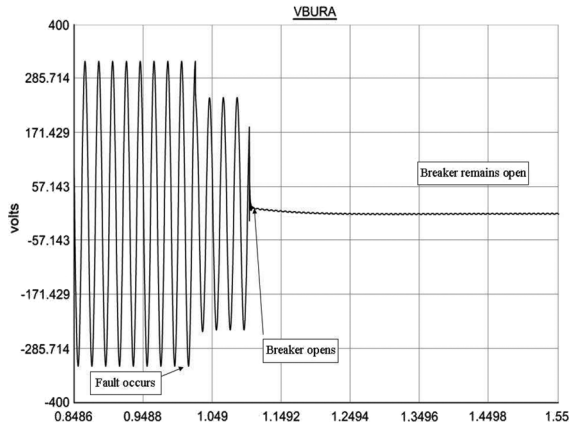

Fig. 9. Typical real-time response to a permanent fault.

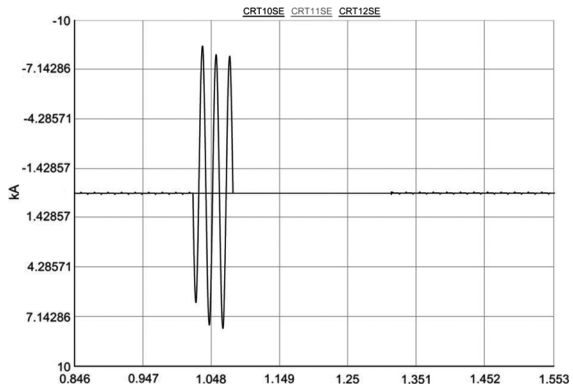

Fig. 10. Typical response to a transient fault, three-phase line currents.

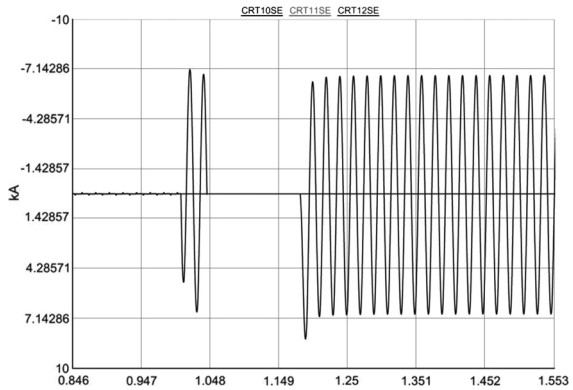

Fig. 11. Real-time response to a forced early reclose decision,three-phase line currents.

The benefit to the system is best viewed through the short-circuit currents sustained on the transmission line. These can be seen in Figs. 10 and 11. With reference to Fig. 10, when the fault occurs, there is a large per-unit short-circuit current on the faulted phase. This then collapses to zero when the circuit breaker isolates this phase. Following the reclose event, a healthy short-circuit current is re-established.

Fig. 11 shows the line currents when the autoreclosing algorithm is bypassed and reclosing is forced before arc extinction. In this case, the primary arc reignites and large fault currents recur. A similar sequence of events occurs in the case of reclosing onto a permanent fault. Although in practice, the protection would soon retrip the breaker following an erroneous reclose, sustaining a second fault is nonetheless hugely detrimental to the system. Ohmic heat is unlikely to dissipate in this time and, therefore, the fault damage is likely to be at least doubled. A comparison of the line currents between Figs. 10 and 11 directly shows the benefit of intelligent autoreclosing.

In some cases, fast autoreclosing has been shown to enhance transient stability. However, it should be noted that transient stability is not a concern in this system, especially when considering single-phase-to-ground faults. In the first instance, power transfer through a double-circuit, 132-kV 30-km line, in an interconnected system is limited by thermal limits rather than transient stability limits. A study of the rotor angle for a single-phase-to-ground fault also shows that the system can sustain this fault condition indefinitely without losing stability.

With reference to Table I, the tests on test cases A were 100% successful, in that for every transient test case, the algorithm recognized the extinction of the secondary arc and safely reclosed, and for every permanent case, autoreclosure was blocked. It can therefore be concluded that this algorithm is robust to the presence of wind farms, at least in the context of this system model.

Some time after these tests were completed, the algorithm was tested on a different primary system, the parameters varied as per Table I, B test cases. This was a 50-km, 400-kV twin-circuit line typical of the U.K. transmission system. The wind farm models were not present in these test cases. The main difference in this system was increased secondary arcing energy due to the increased system voltage. With no changes, the algorithm performed poorly. This was, at first, attributed to poor ANN response, the assumption being that they required retraining for a different primary system. However, further investigation revealed that poor performance was due to the saturation of input levels on the hard limiter, described by (2) (Section IV), confusing the network output. When the input level from the CVT signal was scaled to 50% of that of the 132-kV input level, the algorithm was 100% successful in all 140 tests. This indicates that the input scaling and clipping stage is as crucial as the neural networks and is an area for further work.

X. Conclusion

An accurate, real-world primary system model has been built, together with a versatile relay development platform. Using this platform, an adaptive autoreclosing algorithm has been developed and demonstrated in real time. Extensive tests reveal that the algorithm is 100% successful in the context of this system and is not sensitive to DFIG-based wind generation. A second test suggests that subject to proper input scaling, the algorithm is robust to other transmission systems. However, further work on a whole range of system configurations, combined with real-world fault data, is required to confirm this last conclusion.

Acknowledgment

The authors would like to thank their colleague B. Ross for his help and advice, P. Forsyth and his colleagues at RTDS technologies, J. Henderson at Innovative Integration, and J. Owen, K. Ollington, and T. Bigg at Entegra DSP.

REFERENCES

[1] Areva T&D, The Network Protection and Automation Guide. 2008. [Online]. Available: www.alstom.com/grid/NPAG

[2] D. S. Fitton, R. W. Dunn, R. K. Aggarwal, A. T. Johns, and A. Bennett, "Design and implementation of an adaptive single pole autoreclosure technique for transmission lines using artificial neural networks," *IEEE Trans. Power Del.*, vol. 11, no. 2, pp. 748–756, Apr. 1996.

[3] H. Khorashadi-Zadeh and Z. Li, "Transmission line single phase auto reclosing scheme based on wavelet transform and adaptive fuzzy neuro inferences system," in *Proc. 39th North Amer. Power Symp.*, Las Cruces, NM, 2007, pp. 43–48.

[4] V. V. Terzija and Z. M. Radojevic, "Numerical algorithm for adaptive autoreclosure and protection of medium-voltage overhead lines," *IEEE Trans. Power Del.*, vol. 19, no. 2, pp. 554–559, Apr. 2004.

[5] I. P. Gardiner and J. Ramsden, "On site experience of an adaptive autoreclose relay for ovehead lines," in *Proc. Inst. Elect. Eng. Conf. Publ. Develop. Power Syst. Protect.*, Nottingham, U.K., 1997, pp. 377–380.

[6] Brit. Wind Energy Assoc., British Wind Energy Association Official Website, 2008. [Online]. Available: http://www.bwea.com

[7] S. P. Le Blond and R. K. Aggarwal, "Impact of wind farms on electromagnetic transients on 132 kV network with particular reference to fault detection, CIRED,. Prague, Czech Republic, 2009.

[8] S. P. Le Blond and R. K. Aggarwal, "Design of adaptive autoreclosure schemes for 132 kV network with high penetration of wind: Part 1—Real time modeling," presented at the IEEE Power Energy Soc. Transm. Distrib. Conf. Expo., New Orleans, LA, 2010.

[9] D. Fitton, "A neural network based adaptive single pole autoreclose technique," Ph.D. dissertation, Dept. Electron. Elect. Eng., Univ. Bath, Bath, U.K., 1995.

[10] A. T. Johns, R. K. Aggarwal, and Y. H. Song, "Improved techniques for modelling fault arcs on faulted EHV transmission systems," *Proc. Inst. Elect. Eng., Gen., Transm. Distrib.,*, vol. 141, no. 2, p. 6, 1994.

[11] Y. H. Song, R. K. Aggarwal, and A. T. Johns, "Digital simulation of fault arcs on long-distance compensated transmission-systems with particular reference to adaptive autoreclosure," *Eur. Trans. Elect. Power Eng.*, vol. 5, pp. 315–324, 1995.

[12] Z. Q. Bo, R. K. Aggarwal, A. T. Johns, B. H. Zhang, and Z. Y. Ge, "New concept in transmission line reclosure using high frequency fault transients," in *Proc. Inst. Elect. Eng., Gen. Transm. Distrib.*, 1997, vol. 144, pp. 351–356.

[13] J. Giesbrecht, D. S. Ouellette, and C. F. Henville, "Secondary arc extinction and detection—Real and simulated," presented at the Develop. Power Syst. Protect., Glasgow, U.K., 2008.

[14] A. T. Johns and R. K. Aggarwal, "Digital simulation of faulted EHV transmission lines with particular reference to very high speed protection," *Proc. Inst. Elect. Eng. London*, vol. 123, no. 4, pp. 353–359, 1976.

[15] S. Le Blond, "Intelligent autoreclosing for systems with high penetration of wind with real time modelling, development and deployment," Ph.D. dissertation, Dept. Electron. Elect. Eng., Univ. Bath, Bath, U.K, 2011.

Simon P. Le Blond (M'09) received the B.Sc. (Hons.) degree in physics from the University of Southampton, Southampton, U.K., in 2004, and the Ph.D. degree in electrical and electronic engineering from the University of Bath, Bath, U.K.

His main research interests are real-time power system simulation, power system transients, as well as power system protection and AI techniques applied to power systems. He begins his engineering career with TRL of Toshiba Research Europe Ltd.

Raj Aggarwal (SM'91) received the B.Eng. and Ph.D. degrees in electronics and electrical engineering and the D.Eng. degree for his original and outstanding contribution to electrical power systems from the University of Liverpool, Liverpool, U.K., in 1970, 1973, and 2005, respectively.

He then joined the University of Bath, Bath, U.K., where he is currently Professor of Electrical Engineering and Head of the Electrical Power and Energy Systems Group, Department of Electronic and Electrical Engineering.

Dr. Aggarwal is/has been on several Institute of Engineering and Technology and CIGRÉ committees and has been a member of the EPSRC Scientific Advisory committee on energy. He has published many technical papers and is the recipient of several Institute of Engineering and Technology premium awards for papers published.